Eur. Phys. J. C (2026) 86:211
https://doi.org/10.1140/epjc/s10052-026-15375-y

THE EUROPEAN PHYSICAL JOURNAL C

Regular Article - Theoretical Physics

New agegraphic dark energy in loop quantum cosmology: a quantum gravitational perspective on dark energy evolution

Sayani Maity[1,a], **Aritra Sanyal**[2,b], **Prabir Rudra**[3,c]

[1] Department of Mathematics, Sister Nivedita University, DG-1/2, Action Area 1, New Town, Kolkata 700 156, India
[2] Department of Mathematics, Jadavpur University, Kolkata 700 032, India
[3] Department of Mathematics, Asutosh College, Kolkata 700 026, India

Received: 27 October 2025 / Accepted: 29 January 2026

Abstract In this work, we explore the new agegraphic dark energy model within the framework of Loop Quantum Cosmology (LQC). A quantum gravitational perspective on the dark energy evolution is explored. A combination of cold dark matter and dark energy in the form of New Agegraphic dark energy is considered with LQC as the background gravity theory. Both the interacting and non-interacting scenarios between dark energy and matter are considered. Various cosmological parameters, like the equation of state parameter, deceleration parameter, and statefinder parameters, are studied. The squared speed of sound is investigated to get an idea about the stability of the system. An observational data analysis using recent cosmological data and the Markov chain Monte Carlo algorithm is performed to constrain the free parameter space of the model. Our findings imply that the interaction of loop quantum effects with agegraphic dark energy offers a nonsingular origin scenario and a theoretically sound and observationally compatible explanation of the universe's late-time acceleration.

Contents

1 Introduction

In recent years, cosmology has undergone a major transformation driven by strong observational evidence from multiple sources, confirming that the universe is expanding at an accelerating rate [1–3]. This remarkable discovery has been supported by diverse and independent datasets, including observations of Type Ia supernovae [1–3], the large-scale matter distribution, temperature fluctuations in the Cosmic Microwave Background Radiation (CMBR), data from the WMAP mission [4,5], and measurements of Baryon Acoustic Oscillations (BAO) [6–8]. These observations have provided strong evidence that the universe is predominantly influenced by two enigmatic components: dark matter (DM) and dark energy (DE) [9,10]. While DE is responsible for the universe's current accelerated expansion, DM helps account for galaxy rotation curves and the formation of cosmic structures. In dark energy models, the accelerated expansion is often addressed by modifying the energy-momentum tensor

[a] e-mail: sayani.office88@gmail.com
[b] e-mail: aritrasanyal1@gmail.com
[c] e-mail: prudra.math@gmail.com (corresponding author)

Published online: 03 March 2026

(EMT), which appears on the right-hand side of Einstein's field equations. Conversely, modified gravity theories focus on changing the geometric side, i.e., the left-hand side of these equations. Despite these approaches, a fully unified theory that can simultaneously explain the accelerated expansion of the universe, early-universe issues, structure formation, DM, and other fundamental problems remains elusive. A crucial step toward such a theory involves incorporating quantum effects into gravity. Quantum gravity aims to merge general relativity with the principles of quantum mechanics, although a complete theory has not yet been realized. Among the various proposals grounded in quantum gravity, the Holographic dark energy (HDE) [11,12] and Agegraphic dark energy (ADE) [13,14] models stand out as potential explanations for the universe's late-time acceleration. These models provide a broader theoretical framework to tackle major cosmological challenges, including the cosmological constant problem [15–19], and the cosmic coincidence problem [10,17–19]. These problems have been studied in the background of different modified gravity theories [20–22].

The ADE framework stems from quantum mechanics, particularly the uncertainty principle, and integrates gravitational effects from general relativity (GR). It explains DE through changes in spacetime and matter content as governed by the universe. Based on the idea of quantum fluctuations in space-time, Karolyhazy and his collaborators [23–25] proposed that in Minkowski space-time, the measurement of a time interval t cannot be made with precision better than

$$\delta t = \gamma t_p^{\frac{2}{3}} t^{\frac{1}{3}}, \tag{1.1}$$

where t_p is the reduced Planck time and γ is a dimensionless constant of order one. Maziashvili [26,27] suggested that the quantum energy density arising from metric fluctuations in Minkowski space-time can be estimated using this uncertainty relation combined with the time-energy uncertainty principle. Both Maziashvili [26,27] and Sasakura [28] independently derived the expression for the energy density of these fluctuations as

$$\rho_D \sim \frac{1}{t_p^2 t^2} \sim \frac{M_P^2}{t^2} \tag{1.2}$$

where $M_P^2 = (8\pi G)^{-1}$ is the reduced Planck mass. This energy density is interpreted as that of dark energy, specifically in the context of the Agegraphic Dark Energy (ADE) model. The original ADE model, introduced by Cai [13], was aimed at understanding the accelerated expansion of the universe. It defines the energy density as

$$\rho_D = 3n^2 M_P^2 T^{-2}, \tag{1.3}$$

where T represents the age of the universe, M_P is the Planck mass, and $3n^2$ accounts for certain uncertainties. Despite its elegance, the original ADE model has significant dynamical problems, particularly in the early cosmic era. The cosmos has a very short age T in the matter-dominated era. Hence $\rho_D \sim 1/T^2$ becomes very large. Accordingly, dark energy would take over too soon, defying the established matter-dominated phase that is required for the creation of structures. To put it briefly, the proper cosmic evolution sequence cannot be naturally reproduced by ADE. Furthermore, an incorrect scaling of dark energy with scale factor a is predicted by the ADE model. Conflict with observational data and structural growth results from the equation of state ω_D staying too near the zero level in the past. The model becomes non-local in time when T is defined as the universe's whole age since the energy density is dependent on the universe's entire previous history, which is a little unphysical in dynamical cosmology.

To address this, Wei and Cai [29] introduced the new Agegraphic dark energy (NADE) model, which substitutes the universe's age with conformal time η. This revised model also naturally resolves the coincidence problem [30]. A notable advantage of the NADE model is that it involves the same number of parameters as the ΛCDM model (which includes the cosmological constant and cold dark matter), making it more economical compared to other dynamical dark energy models. Additionally, the NADE model has demonstrated good agreement with observational data [31–33]. For further analysis, see Refs. [34–36]. In Ref. [37], the NADE model have been explored in the context of $f(P)$ cubic gravity.

In Ref. [38], entropy-corrected holographic and new agegraphic dark energy models are studied within the framework of generalized Rastall gravity using two types of scale factors, one representing a future singularity and the other an initial singularity. For each model, key cosmological parameters, including the Hubble parameter, deceleration parameter, and equation of state, are computed, and their cosmological implications are analyzed. The phenomenon of accelerated expansion of a flat D-dimensional fractal Universe has been explored by examining non-linear interactions between cold dark matter and the dark energy models, including Tsallis, Renyi, and Sharma-Mittal HDE and NADE in Ref. [39]. In Ref. [40], the authors have studied the thermodynamic framework governing the interaction between new agegraphic dark energy (NADE) and dark matter (DM) in an anisotropic universe and derived the corresponding expressions for the entropy variations of these dark energy components. In Ref. [41], new agegraphic dark energy model is reconstructed within the $f(Q)$ gravity framework, assuming a power-law scale factor in flat Friedmann-Robertson-Walker (FRW) spacetime. The analysis of $r-s$ plane, along with stability tests, reveals a quintessence phase and shows that the model effectively addresses the cosmic coincidence problem. In Ref. [42], new agegraphic dark energy model is investi-

gated in the framework of $f(Q,T)$ gravity in a flat FRW universe with a power-law scale factor. The model exhibits a quintessence phase, which corresponds to the Chaplygin gas behavior in the $r-s$ plane. In Ref. [43], a comprehensive global fit analysis of the new agegraphic dark energy (NADE) model in a non-flat universe is carried out using the Markov chain Monte Carlo method, incorporating the full CMB power spectrum from WMAP 7-year data, SNIa observations from the Union 2.1 sample, BAO measurements from SDSS DR7 and WiggleZ surveys, and the latest H_0 estimates from HST.

Loop Quantum Cosmology (LQC) [44,45] is the cosmological adaptation of Loop Quantum Gravity (LQG) [46,47], a theoretical framework that seeks to quantize gravity using a non-perturbative and background independent approach. LQG is a leading non-perturbative and background-independent approach to quantum gravity, aimed at resolving the limitations of GR at the Planck scale [48]. In scenarios like black holes (BH) and the early universe, where curvature becomes extreme, classical GR breaks down, necessitating a quantum theory of gravity. In black hole physics, LQG suggests that quantum gravity effects become significant not only at the singularity but at a finite radius before it, as seen in modifications to the classical Schwarzschild solution. These corrections arise from expressing the Hamiltonian in terms of holonomies and fluxes core elements of LQG, rather than the classical connection. This leads to effective equations of motion that incorporate quantum effects via Planck-scale loops, as demonstrated in spherically symmetric spacetimes such as the Lemaitre-Tolman-Bondi (LTB) dust collapse model [49].

In cosmology, LQG leads to LQC, which applies LQG principles under cosmological symmetry reductions. LQC resolves the classical big bang singularity by replacing it with a quantum "bounce" due to repulsive effects of quantum geometry at high curvature. This bounce prevents the divergence of curvature invariants and provides a framework for exploring the early universe, including the emergence of inflation. While the inflationary paradigm effectively explains the observed structure of the universe and CMB anisotropies, it does not solve the singularity problem or extend GR to the Planck regime. LQC, on the other hand, addresses these by providing a singularity-free beginning and studying the naturalness and probability of inflation post-bounce. However, defining initial conditions and a proper measure in quantum gravity remains a challenge in determining the likelihood of inflationary scenarios.

In LQC, Planck units are used with $c=G=1$, and the fundamental time unit is the Planck second. LQC reformulates cosmological dynamics by encoding spatial geometry in terms of the volume $V\propto a^3$ of a fiducial cell, rather than the scale factor a itself. The variable b, conjugate to V, is related to the Hubble parameter $H=\dot{a}/a$ through $b=\gamma H$ in classical solutions, where $\gamma\approx 0.24$ is the Barbero–Immirzi parameter fixed by black hole entropy calculations. However, LQC modifies the classical Einstein dynamics and gives a singularity free evolution of the universe. The effective Hubble parameter becomes

$$H=\frac{1}{2\gamma\lambda}\sin(2\lambda b)\approx 0.93\,\ell_{\rm Pl}^{-1}\sin(2\lambda b), \tag{1.4}$$

where $\lambda^2\approx 5.2\,\ell_{\rm Pl}^2$ represents the area gap, the smallest non-zero eigenvalue of the area operator in LQG.

In LQC, the modified Friedmann equation takes the form:

$$H^2=\frac{1}{3m_{pl}^2}\rho\left(1-\frac{\rho}{\rho_c}\right), \tag{1.5}$$

where $H=\frac{\dot{a}}{a}$ is the Hubble parameter, and a is the cosmological scale factor. The total energy density $\rho=\rho_m+\rho_D$ represents the sum of the densities of cold dark matter (CDM) and DE. The critical density $\rho_c=\frac{\sqrt{3}}{16\pi^2\gamma^3G^2\hbar}$ defines the maximum energy scale before quantum effects dominate, where γ is the Barbero–Immirzi parameter. LQC predicts that cosmic singularities such as the Big Bang, Big Rip, and other future singularities can be resolved in the semi-classical regime. Furthermore, quantum corrections significantly modify the standard FRW cosmology, leading the universe to undergo a cosmic bounce followed by eternal oscillations. With the critical energy density $\rho_{\rm c}\approx 0.41\,\rho_{\rm Pl}$, the modified Friedmann equation in LQC reveals that: At low densities $\rho\ll\rho_c$, quantum effects vanish and classical GR is recovered. At high densities $\rho\to\rho_c$, quantum geometry effects become significant and modify spacetime dynamics drastically. In contrast to GR, where a positive matter density implies continuous expansion or contraction, the LQC framework predicts a quantum bounce. When the energy density reaches ρ_c, the universe undergoes a smooth transition from a contracting phase to an expanding phase, avoiding the classical big bang singularity. LQC has been studied extensively in the literature. In Ref. [50], Pilgrim Dark Energy has been investigated within an LQG-inspired cosmology using its generalized ghost version. Other recent developments in LQC can be found in [51–56].

The NADE model successfully relates dark energy to quantum fluctuations of spacetime and the conformal age of the universe, and its standard formulation lacks a direct quantum gravitational foundation. LQG, on the other hand, offers a background-independent and non-perturbative quantization of spacetime geometry, introducing natural corrections to the early and late-time cosmic dynamics. Here we are motivated to study the cosmological dynamics of NADE in a universe described by LQG. Embedding the NADE model in the LQG framework provides an opportunity to explore

how quantum geometric effects modify dark energy behavior, potentially resolving cosmological singularities, refining late-time acceleration mechanisms, and offering a unified description of the universe's evolution from quantum to classical regimes. The paper is organized as follows: in Sect. 2, we discuss the basic equations of NADE in LQC in both non-interacting and interacting scenarios between CDM and DE. Section 3 deals with the study of the basic cosmological parameters. In Sect. 4, we explore the statefinder parameters of the model. Section 5 is dedicated to a comprehensive observational data analysis of the setup leading to the constraining of the parameter space. Finally, the paper ends with a discussion and conclusion in Sect. 6.

2 NADE in the framework of LQC

In this section, we explore the basic setup involving an interaction between cold dark matter and the New Agegraphic Dark Energy model within the context of LQC. The energy density of the NADE model is given by [29]

$$\rho_D = 3n^2 m_{pl}^2 \eta^{-2} \tag{2.1}$$

where n is the uncertainty parameter and m_{pl} is the reduced Planck mass. The conformal time η is given by

$$\eta = \int_0^t \frac{dt}{a} = \int_0^a \frac{da}{Ha^2} \tag{2.2}$$

Here, we will adopt a power-law form for the scale factor a as presented in [57,58]

$$a(t) = b_0 t^{\beta}, \quad \beta > 0 \tag{2.3}$$

where b_0 is the current value of the scale factor and β is the power-law exponent. This form of the scale factor implies an initial Big Bang singularity but does not lead to any finite-time future singularities. In LQC, the initial big-bang singularity is indeed resolved and replaced by a non-singular quantum bounce. But the chosen power-law form of the scale factor implies an initial Big Bang singularity. These may seem to be contradictory assumptions, but actually, they are not. In the present work, however, our focus is on the late-time, post-bounce regime, where quantum geometric effects become subdominant, and the effective dynamics smoothly approach those of classical cosmology. In this regime, the power-law form of the scale factor serves as a well-motivated and widely used approximation that captures the accelerated expansion driven by dark energy. So this ansatz is fairly logical to consider. Various studies have investigated the cosmological implications of such scale factors in the context of different modified gravity theories [41,42]. In Ref. [59], Zhu et al. assumed a power-law evolution to test whether a simple constant-exponent expansion can reproduce the observed acceleration of the Universe. They used galaxy cluster data to constrain the power-law parameter showing that power-law cosmology provides a viable alternative to CDM at late times. In Ref. [60], Kumar adopted power-law form of scale factor to examine observational limits on the Hubble and deceleration parameters. The model's simplicity enables analytical comparison with supernova and Hubble data, offering insight into the history of cosmic expansion. In Ref. [61], Sharif and Waheed used power-law forms for both the scale factor and scalar field in Brans–Dicke theory to obtain exact anisotropic cosmological solutions. This approach simplifies the field equations and helps study scalar field effects on cosmic dynamics. In Ref. [62], Singh et al. considered power-law form of scale factor in $f(R, G)$ gravity to explore cosmic acceleration and thermodynamical consistency. The power-law assumption allows analytical treatment of modified field equations and effectively describes different expansion phases. For this form of scale factor, the energy density of the NADE model in terms of the redshift z reads

$$\rho_D = 3n^2 m_{Pl}^2 (1-\beta)^2 b_0^{\frac{2}{\beta}} (1+z)^{\frac{2}{\beta}-2} \tag{2.4}$$

Now we will consider non-interacting and interacting scenarios between CDM and DE and study the setups separately.

2.1 Non-interacting case

If we consider that there is no interaction between DE and CDM and both are conserved separately, the respective conservation equations of the components yield

$$\dot{\rho_m} + 3H\rho_m = 0 \tag{2.5}$$

and

$$\dot{\rho_D} + 3H\rho_D(1+\omega_D) = 0 \tag{2.6}$$

where ρ_m is the energy density of CDM, and $\omega_D = p_D/\rho_D$ is the equation of state (EoS) parameter of DE. Solving equation (2.5) we get

$$\rho_m = \rho_{m_0}(1+z)^3 \tag{2.7}$$

where ρ_{m0} is the current energy density of CDM. The FRW equations of LQC (Eq. 1.5) with NADE and CDM can be given by

$$H^2(z) = (1+z)^3 \left[b_0^{\frac{2}{\beta}} n^2 (1-\beta)^2 (1+z)^{\frac{2}{\beta}-5} + \Omega_{m0} H_0^2 \right] \times \left[1 - \frac{3}{\rho_c} m_{pl}^2 (1+z)^3 \left(b_0^{\frac{2}{\beta}} n^2 (1-\beta)^2 (1+z)^{\frac{2}{\beta}-5} \right. \right.$$

$$+\Omega_{m0}H_0^2\Big)\Big] \tag{2.8}$$

Differentiating Eq. (1.5) and exploiting Eqs. (2.4) and (2.7) we get

$$\frac{\dot{H}}{H^2} = \frac{H_0^2}{H^2}\left\{\frac{n^2 b_0^{\frac{2}{\beta}}}{\beta H_0^2}(1-\beta)^3(1+z)^{\frac{2}{\beta}-2} - \frac{3}{2}\Omega_{m_0}(1+z)^3\right\} \times\left\{1 - \frac{6H_0^2 m_{pl}^2}{\rho_c}\left(\Omega_{m_0}(1+z)^3 + \frac{n^2}{H_0^2}b_0^{\frac{2}{\beta}}(1-\beta)^2(1+z)^{\frac{2}{\beta}-2}\right)\right\} \tag{2.9}$$

where $\Omega_{m_0} = \frac{\rho_{m0}}{3m_{pl}^2 H_0^2}$ is the dimensionless matter density parameter, and H_0 is the present value of the Hubble parameter.

2.2 Interacting case

Next, we consider an interaction between the NADE and CDM. In this case, the continuity equations for matter and DE are respectively given by

$$\dot{\rho_m} + 3H\rho_m = Q, \tag{2.10}$$

and

$$\dot{\rho_D} + 3H\rho_D(1+\omega_D) = -Q. \tag{2.11}$$

Here, Q is a dynamic quantity that acts as the interaction term between CDM and NADE. A coupling between DE and DM is a possible approach to alleviate the cosmic coincidence problem. The presence of such an interaction can substantially modify the background dynamics and stability of the universe, leading to evolution distinct from the Standard Cosmological Model. In Ref. [63] Yang et al. analyzed large-scale inhomogeneous perturbations and the associated instabilities in interacting DE models, demonstrating that the interaction term can significantly affect the stability of cosmological perturbations. The phase-space dynamics of the FRW universe containing various interacting and non-interacting fluids were investigated by Odintsov et al. in [64], where the interaction was shown to shift the critical points and alter the late-time attractor behavior. A comprehensive discussion of linear and non-linear interactions in the dark sector, including theoretical motivations and phenomenological implications, has been presented by Bolotin et al. [49], where the authors emphasized that interacting scenarios can yield cosmological dynamics very different from those predicted by the standard cosmological model. Other studies, such as [65–67] provide broader theoretical backgrounds through modified gravity and holographic or agegraphic dark-energy frameworks, which often serve as foundations for introducing interaction terms. These investigations highlight that allowing interactions between DE and DM not only provides a plausible mechanism for addressing the coincidence problem but also enriches the cosmological dynamics, offering potential explanations for various late-time phenomena.

Typically, three commonly used forms of Q are considered widely in the literature. They are given by

$$Q_1 = 3\delta H\rho_D, \quad Q_2 = 3\delta H(\rho_m + \rho_D), \quad Q_3 = 3\delta H\rho_m \tag{2.12}$$

where δ is the interaction constant representing the strength of the energy exchange between DM and DE. In this study, we adopt the third form, Q_3, which has been widely used in the literature to model energy transfer under various cosmological constraints. The sign of the coupling constant δ determines the direction of energy flow. A positive value indicates that DE decays into DM, whereas a negative value implies that DM transforms into DE. Observational data and theoretical investigations generally favor the scenario where DE decays into DM. In [68] Early joint fits (SNe + CMB shift + BAO) found δ to be small and often consistent with a near-zero value; e.g. Guo et al. reported $-0.08 < \delta < 0.03$ for a constant coupling.

By solving Eq. (2.10) using the interaction term Q_3, we obtain

$$\rho_m = \rho_{m_0}(1+z)^{3(1-\delta)} \tag{2.13}$$

The corresponding FRW equation changes to

$$H^2(z) = (1+z)^{3-3\delta}\left[b_0^{\frac{2}{\beta}} n^2(1-\beta)^2(1+z)^{\frac{2}{\beta}-5+3\delta} + \Omega_{m0}H_0^2\right] \times\left[1 - \frac{3}{\rho_c}m_{pl}^2(1+z)^{3-3\delta} \left(b_0^{\frac{2}{\beta}} n^2(1-\beta)^2(1+z)^{\frac{2}{\beta}-5+3\delta} + \Omega_{m0}H_0^2\right)\right] \tag{2.14}$$

Differentiating (1.5) and exploiting (2.11) and (2.13) we get

$$\frac{\dot{H}}{H^2} = \frac{H_0^2}{H^2}\left[\frac{n^2 b_0^{\frac{2}{\beta}}}{\beta H_0^2}(1-\beta)^3(1+z)^{\frac{2}{\beta}-2} + \frac{3}{2}(\delta-1)\Omega_{m_0}(1+z)^{3-3\delta}\right] \times\left[1 - \frac{6H_0^2 m_{pl}^2(z+1)^{1-3\delta}}{\rho_c} \left(\Omega_{m_0} + \frac{n^2}{\beta H_0^2}b_0^{(\frac{2}{\beta})}(1-\beta)^2(1+z)^{\frac{2}{\beta}-3+3\delta}\right)\right] \tag{2.15}$$

3 Cosmological parameters

In this section, we will study the cosmology of NADE in LQC that we have developed in the previous section. To do this, we will explore the basic cosmological parameters like the EoS parameter, the deceleration parameter, etc.

3.1 EoS parameter

We examine the cosmological implications of the equation of state (EoS) parameter, defined as

$$\omega_D = \frac{p_D}{\rho_D} \tag{3.1}$$

where ρ_D, p_D denote the dark energy density and pressure, respectively. The different phases of the universe correspond to various values of ω_D. If $\omega_D = 0$, it corresponds to a non-relativistic matter-dominated era (pressure-less dust). For the quintessence phase, we have $-1 < \omega_D < -\frac{1}{3}$. For the ΛCDM and phantom phase we have $\omega_D = -1$ and $\omega_D < -1$ respectively. If ω_D crosses over from $\omega_D > -1$ to $\omega_D < -1$ (i.e., the model crosses the phantom divide line $\omega_D = -1$), the model exhibits quintom behavior.

3.1.1 Non-interacting case

Exploiting Eqs. (2.4), (2.6) and (3.1) the equation of state parameter reads:

$$\omega_D = -1 - \frac{2}{3}\left(1 - \frac{1}{\beta}\right) \tag{3.2}$$

From the above expression, we see that the equation of state takes a constant value for the non-interacting case, and is not dependent on the redshift z. In this case, the equation-of-state parameter ω_D remains constant due to the assumed power-law form of the scale factor. This is totally an artifact of the ansatz. What matters is that this is not an issue for the late-time evolution of the universe, considering that a small cosmological constant can do this effectively. Now, for this case, we can realize the quintessence phase for $1/2 < \beta < 1$. The ΛCDM phase can be realized for $\beta = 1$, and for $\beta = 2/5$, we get the pressureless dust. For $\beta > 1$, we get the phantom universe. For $\beta > 1$, the model formally enters a phantom regime. This phantom behavior can lead to confusion and inconsistency, considering the singularity-free nature of LQC. It is important to emphasize that this phantom-like behavior represents an effective late-time description rather than a true physical instability. In the context of Loop Quantum Cosmology, quantum geometric effects are known to regularize the dynamics and prevent the occurrence of future singularities commonly associated with phantom dark energy. Since the present analysis focuses on the post-bounce, dark energy-dominated era, the emergence of an effective phantom phase remains compatible with the non-singular nature of LQC. Moreover, the realization of phantom-like behavior in the LQC framework is totally an emergent and geometric phenomenon, without any pathologies. In [69], the author explicitly shows that near the bounce, the quantum geometric modifications lead to a phase where a canonical scalar field mimics the dynamics of a phantom field and vice versa. In [70], the authors show super-inflation for tachyon matter in LQC, which is another instance of an effective phantom-like phase due to quantum corrections. In [71], Li et al. discuss the universal features of effective LQC dynamics, including super-inflation post-bounce; while not framed specifically as "phantom," the regime with $\dot{H} > 0$ (super-inflation) has the same effective properties. This discussion shows that a phantom-like regime is possible in LQC. This realization is effective, and not fundamental. It arises from quantum geometric corrections and is totally ghost-free and singularity-free. Therefore, LQC provides a healthy realization of phantom behavior (which is emergent and geometric) without pathologies.

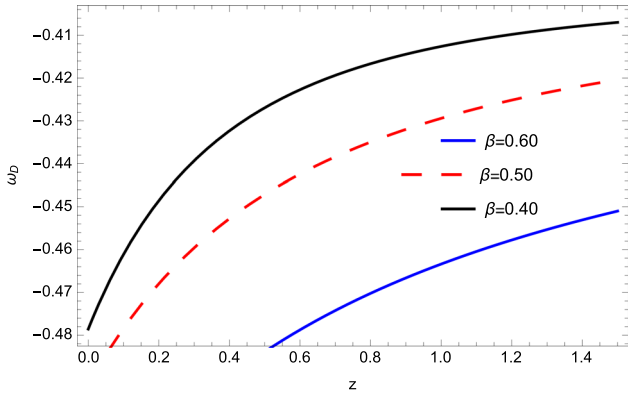

Fig. 1 The figure shows the plot of EoS parameter ω_D against redshift for the interacting case. Other parameters are considered as $H_0 = 69$, $\Omega_{m0} = 0.29$, $b_0 = 0.81$, $\delta = 0.88$ and $n = 0.11$

3.1.2 Interacting case

Using the Eqs. (2.4), (2.11) and (3.1) for the interaction case, the EoS parameter yields

$$\omega_D = -1 - \frac{2}{3}\left(1 - \frac{1}{\beta}\right) - \frac{\delta H_0^2 \Omega_{m0}}{n^2(1-\beta)^2 b_0^{\frac{2}{\beta}}}(1+z)^{(5-\frac{2}{\beta}-3\delta)} \tag{3.3}$$

The plot of ω_D for the interacting case is shown in Fig. 1 for three different values of the parameter β. We see that for all three cases, the model gives quintessence-type behavior in recent times.

3.2 Deceleration parameter

The deceleration parameter, denoted by q, is a dimensionless quantity that describes the rate of change of the cosmic expansion. It indicates whether the expansion of the universe is accelerating or decelerating. It is defined as

$$q = -1 - \frac{\dot{H}}{H^2} \tag{3.4}$$

$q > 0$ indicates a decelerating universe and $q < 0$ presents an accelerating phase of the universe.

3.2.1 Non-interacting case

For the non-interacting case, the deceleration parameter q takes the form

$$\begin{aligned} q &= -1 - \frac{\dot{H}}{H^2} = -1 - \frac{H_0^2}{H^2} \\ &\times \left\{ \frac{n^2 b_0^{\frac{2}{\beta}}}{\beta H_0^2} (1-\beta)^3 (1+z)^{\frac{2}{\beta}-2} - \frac{3}{2}\Omega_{m_0}(1+z)^3 \right\} \\ &\times \left\{ 1 - \frac{6H_0^2 m_{pl}^2}{\rho_c} \right. \\ &\left. \left(\Omega_{m_0}(1+z)^3 + \frac{n^2}{H_0^2} b_0^{\frac{2}{\beta}} (1-\beta)^2 (1+z)^{\frac{2}{\beta}-2} \right) \right\}. \end{aligned} \tag{3.5}$$

The plot of the deceleration parameter q against z for the noninteracting case is drawn in Fig. 2. We see a smooth transition from a decelerating to an accelerating universe around $z \approx 0.5$, which is an observationally favored value.

3.2.2 Interacting case

In this case, the deceleration parameter takes the form

$$\begin{aligned} q &= -1 - \frac{\dot{H}}{H^2} = -1 - \frac{H_0^2}{H^2} \\ &\times \left\{ \frac{n^2 b_0^{\frac{2}{\beta}}}{\beta H_0^2} (1-\beta)^3 (1+z)^{\frac{2}{\beta}-2} + \frac{3}{2}(\delta-1)\Omega_{m_0}(1+z)^{3-3\delta} \right\} \\ &\times \left\{ 1 - \frac{6H_0^2 m_{pl}^2 (z+1)^{1-3\delta}}{\rho_c} \right. \\ &\left. \left(\Omega_{m_0} + \frac{n^2}{\beta H_0^2} b_0^{(\frac{2}{\beta})} (1-\beta)^2 (1+z)^{\frac{2}{\beta}-3+3\delta} \right) \right\} \end{aligned} \tag{3.6}$$

The plot of the deceleration parameter q against z for the interacting case is drawn in Fig. 3. We see a smooth transition from a decelerating to an accelerating universe around $z \approx 0.4$, which is an observationally favored value.

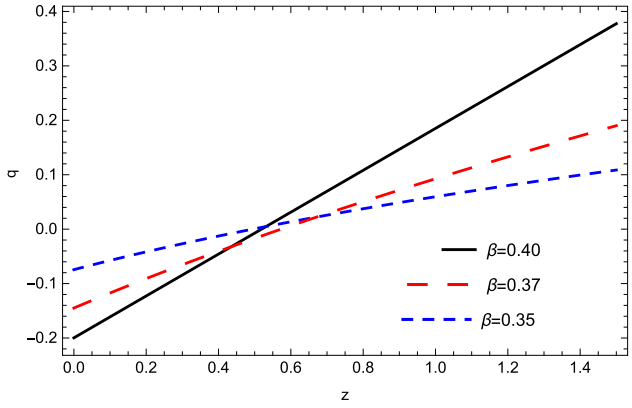

Fig. 2 The figure shows the plot of deceleration parameter against redshift for the non-interacting case. The other parameters are considered as $H_0 = 69$, $\Omega_{m0} = 0.29$, $b_0 = 0.76$ and $n = 0.111$

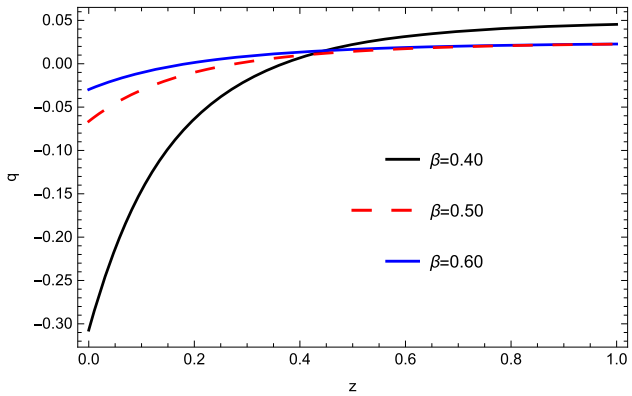

Fig. 3 The figure shows the plot of the deceleration parameter q against redshift z for the interacting case. The other parameters are considered as $H_0 = 69$, $\Omega_{m0} = 0.29$, $b_0 = 0.81$, $\delta = 0.88$ and $n = 0.11$

3.3 Stability analysis: squared speed of sound

Now, we examine the stability analysis of the constructed system through the squared speed of sound, which is defined as the partial derivative of pressure with respect to energy density. The expression for the squared speed of sound reads:

$$v_s^2 = \frac{\dot{p_D}}{\dot{\rho_D}} = \frac{\acute{p_D}}{\acute{\rho_D}} = \omega_D + \acute{\omega_D}\frac{a\beta}{2(\beta-1)}, \tag{3.7}$$

where $(\acute{})$ represents the derivative with respect to scale factor a. The sign of the squared speed of sound determines whether the model is classically stable or unstable. A positive value indicates stability, while a negative value generally signifies instability within the framework of GR. For the non-interacting case, ω_D is constant and hence $\acute{\omega_D}$ will vanish. The corresponding expression for the squared speed of sound is obtained as

$$v_s^2 = \omega_D \tag{3.8}$$

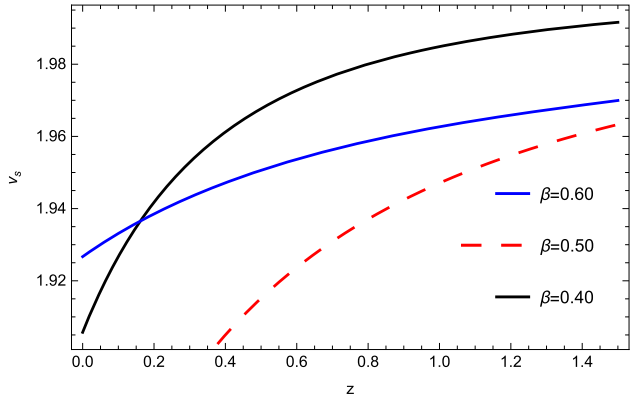

Fig. 4 Squared speed of sound against redshift z for the interacting case. The other parameters are considered as $H_0 = 69$, $\Omega_{m0} = 0.29$, $b_0 = 0.81$, $\delta = 0.88$ and $n = 0.11$

For the interacting case $\omega_D^{'}$ takes the form

$$\omega_D^{'} = -\frac{\delta H_0^2 \Omega_{m0}(3\delta - 5 + \frac{2}{s})}{n^2(1-s)^2 b_0^{\frac{2}{s}}}(1+z)^{6-3\delta-\frac{2}{s}} \tag{3.9}$$

The corresponding squared speed of sound is obtained as

$$v_s^2 = \frac{1}{3}\left(\frac{2}{\beta} - 5\right) - \frac{3\delta\beta(\delta-1)\Omega_{m0}H_0^2}{2n^2(\beta-1)^3 b_0^{\frac{2}{\beta}}}(1+z)^{(5-\frac{2}{\beta}-3\delta)} \tag{3.10}$$

We observe that $v_s^2 = \omega_D$ for the non-interacting case indicates that the model is not classically stable since the current epoch is dominated by quintessence-type dark energy with $\omega_D < -1/3$ (i.e. $v_s^2 < 0$). The plot of v_s^2 against redshift z for the interacting case for different values of β is given in Fig. 4. It is seen that in each of the cases, the constructed model is classically stable throughout the evolution of the universe, since v_s^2 lies in the positive range.

4 Statefinder parameters: $r - s$ plane

Over time, numerous DE models have been introduced to account for the accelerated expansion of the universe, giving rise to the challenge of distinguishing among them. To assess the viability of these models, the statefinder parameters [72,73] are commonly employed. The reason for this is that the statefinder approach may detect differences at higher orders, even in models with quite similar expansion histories. Therefore, the statefinder diagnostic approach is ideally adapted to distinguish between seemingly comparable models since it takes into account higher-order corrections in derivatives of the scale factor. The statefinder parameters are

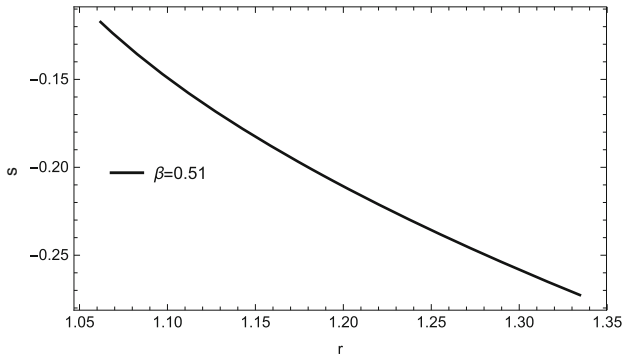

Fig. 5 $r - s$ plane for non-interacting case for $\beta = 0.51$. The other parameters are considered as $H_0 = 69$, $\Omega_{m0} = 0.29$, $b_0 = 0.76$ and $n = 0.111$

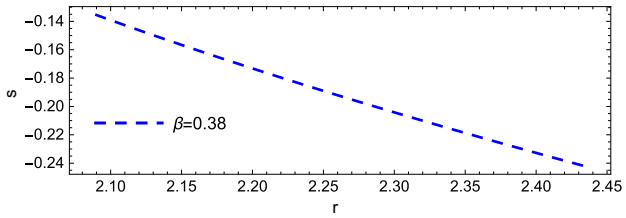

Fig. 6 r-s plane for non-interacting case for $\beta = 0.38$. The other parameters are considered as $H_0 = 69$, $\Omega_{m0} = 0.29$, $b_0 = 0.76$ and $n = 0.111$

expressed as

$$r = \frac{\dddot{a}}{aH^3}, \quad s = \frac{r-1}{3(q-\frac{1}{2})}, \tag{4.1}$$

where q represents the deceleration parameter. In terms of the Hubble and deceleration parameters, the statefinder parameters can be rewritten as

$$r = 2q^2 + q - \frac{\dot{q}}{H}, \quad s = \frac{r-1}{3(q-\frac{1}{2})}. \tag{4.2}$$

These parameters are dimensionless, and the corresponding cosmological plane is known as the $r - s$ plane. The trajectories in this plane indicate how far a given DE model deviates from the ΛCDM limit. The key regions defined by these parameters are: $(r, s) = (1, 0)$ representing the ΛCDM limit, $(r, s) = (1, 1)$ denoting the CDM limit, $s > 0, r < 1$ corresponding to the phantom region, and $s < 0, r > 1$ indicating the quintessence region.

Owing to the complexity of the analytical forms of the parameters r, s, their explicit expressions are omitted. The characteristics of the cosmological $r - s$ plane are analyzed graphically for different values of β for both interacting and noninteracting cases. The plots are given in the Figs. 5, 6 and 7 for the non-interacting case and Figs. 8, 9 and 10 for the interacting case. It is seen that for all the cases, the trajectories of the $r - s$ plane yield a quintessence region ($s < 0, r > 1$).

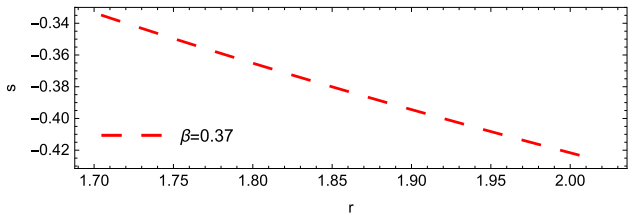

Fig. 7 $r-s$ plane for non-interacting case for $\beta = 0.37$. The other parameters are considered as $H_0 = 69$, $\Omega_{m0} = 0.29$, $b_0 = 0.76$ and $n = 0.111$

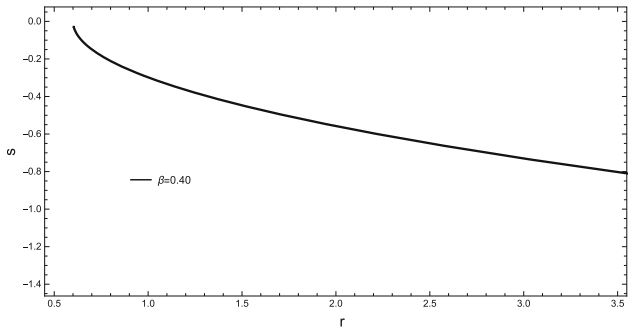

Fig. 8 $r-s$ plane for interacting case for $\beta = 0.40$. The other parameters are considered as $H_0 = 69$, $\Omega_{m0} = 0.29$, $b_0 = 0.81$, $\delta = 0.88$ and $n = 0.11$

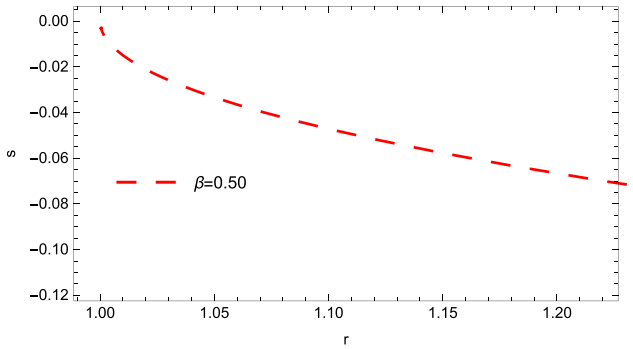

Fig. 9 r-s plane for interacting case for $\beta = 0.50$. The other parameters are considered as $\Omega_{m0} = 0.29$, $b_0 = 0.81$, $\delta = 0.88$ and $n = 0.11$

5 Observational data analysis

In this section, we will perform an observational data analysis for NADE in LQC using some recent observational data and constrain the parameter space.

5.1 Observational data sets and data methodology

Here, the free parameters are estimated using recent observational datasets through a Bayesian statistical framework. The cosmological datasets employed for the analysis include Hubble parameter measurements (HUBBLE), Baryon Acoustic Oscillation (BAO), and Dark Energy Spectroscopic Instrument (DESI) data. The analysis aims to investigate how well

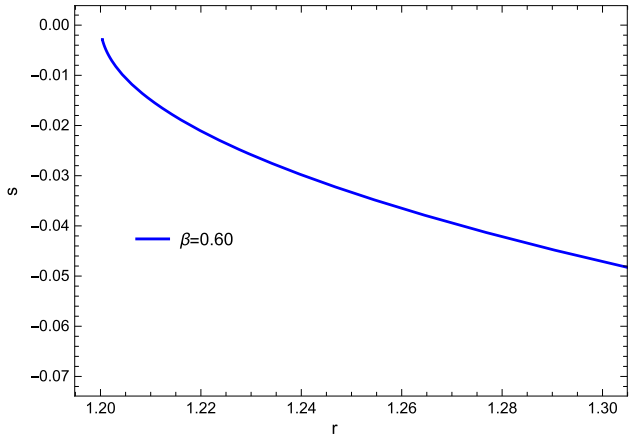

Fig. 10 $r-s$ plane for interacting case for $\beta = 0.60$. The other parameters are considered as $\Omega_{m0} = 0.29$, $b_0 = 0.81$, $\delta = 0.88$ and $n = 0.11$

the model fits these independent data sets as well as their combinations. Below, we discuss in detail the datasets used in the analysis:

- **HUBBLE Data:** We use 32 model-independent measurements of the Hubble parameter $H(z)$, commonly known as Cosmic Chronometers (CC) [74,75]. The covariance matrix used to estimate the likelihood is constructed following the approach described in [76,77]. These data points provide direct constraints on the expansion history of the universe.
- **BAO Data:** The BAO dataset provides constraints on the large-scale structure of the universe through measurements of the baryon acoustic feature imprinted in the matter power spectrum. We use the distance measurements from various galaxy surveys compiled in the DESI and eBOSS analyses [78,79]. The observables considered include D_M/r_d, D_H/r_d, and D_V/r_d, where D_M is the comoving angular diameter distance, D_H is the Hubble distance, and r_d is the comoving sound horizon at the drag epoch.
- **DESI Data:** The Dark Energy Spectroscopic Instrument (DESI) Release II dataset provides high-precision BAO and redshift-space distortion (RSD) measurements across a wide redshift range [80]. These measurements significantly improve constraints on late-time cosmic acceleration and expansion rate, complementing the HUBBLE and BAO datasets.

For parameter estimation, we consider several combinations of observational datasets to assess the robustness of the system. The individual datasets include Hubble, BAO, and DESI measurements. We also analyze their combined forms—Hubble+BAO, Hubble+DESI, BAO+DESI, and the joint dataset Hubble+BAO+DESI—to provide a comprehen-

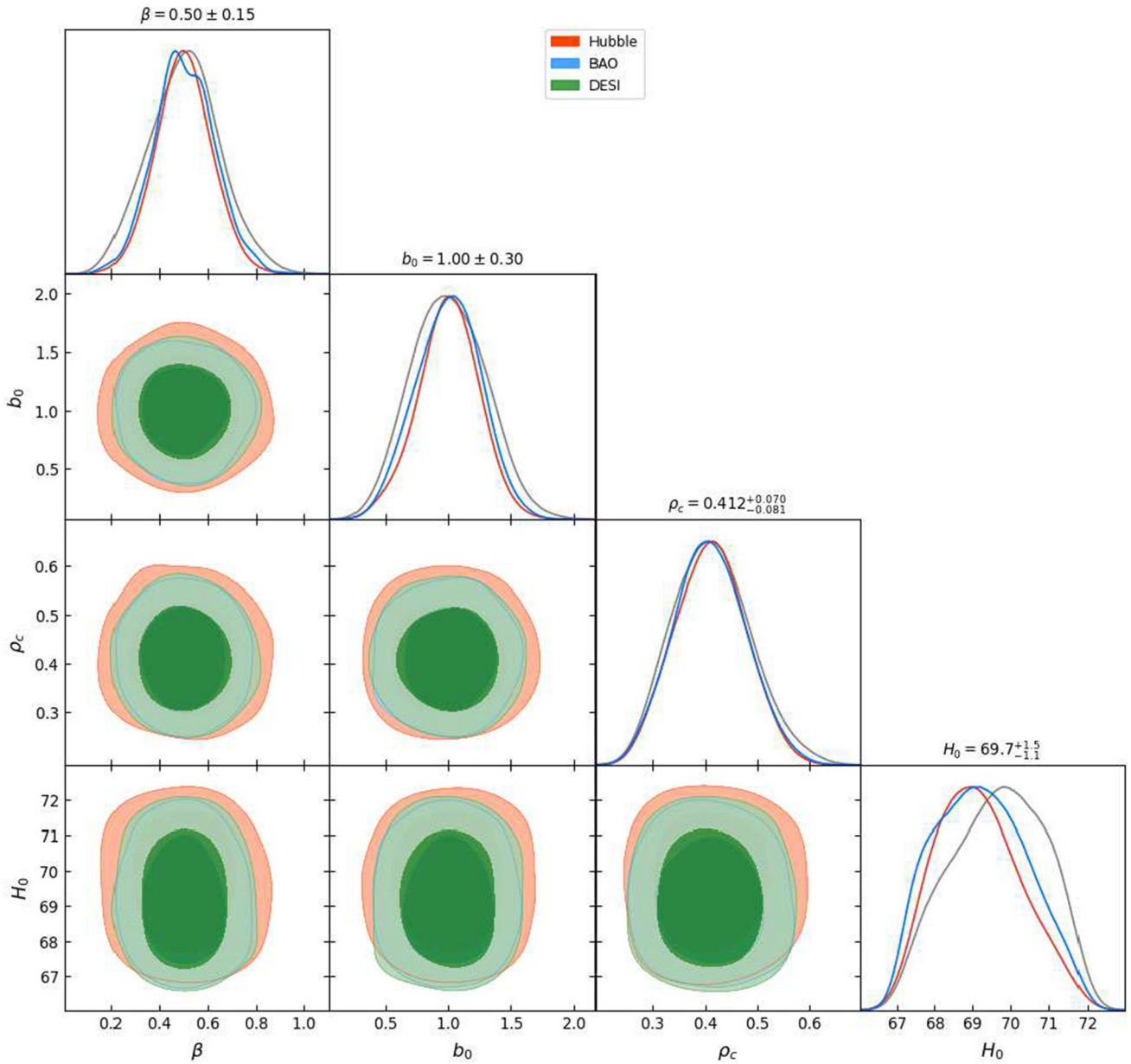

Fig. 11 Joint and marginalized posterior distributions with combinations of datasets Hubble, BAO and DESI for the non-interacting case. The fixed parameters are considered as $m_{pl} = 1$, $\Omega_{m0} = 0.29$, $n = 1.1$

sive evaluation of the model's performance across different observational constraints. Each dataset combination provides independent constraints on the parameters, and the final combined analysis (HUBBLE+BAO+DESI) yields the tightest confidence bounds with the smallest statistical uncertainties. The two-dimensional confidence contours shown in the parameter constraint plots represent the joint probability distributions of the model parameters obtained from the likelihood analysis. The colour scheme of the contour plots follows the standard cosmological convention:

- The light-shaded region corresponds to the 95% confidence level (C.L.), indicating the parameter space within which the true values are expected to lie with 95% probability.
- The dark-shaded region corresponds to the 68% confidence level (C.L.), representing the 1σ range of the best-fit values.

The central black dot in each contour marks the best-fit parameter values, while the surrounding elliptical regions illustrate the covariance between the two fitted parameters. The darker inner contour thus represents the most probable

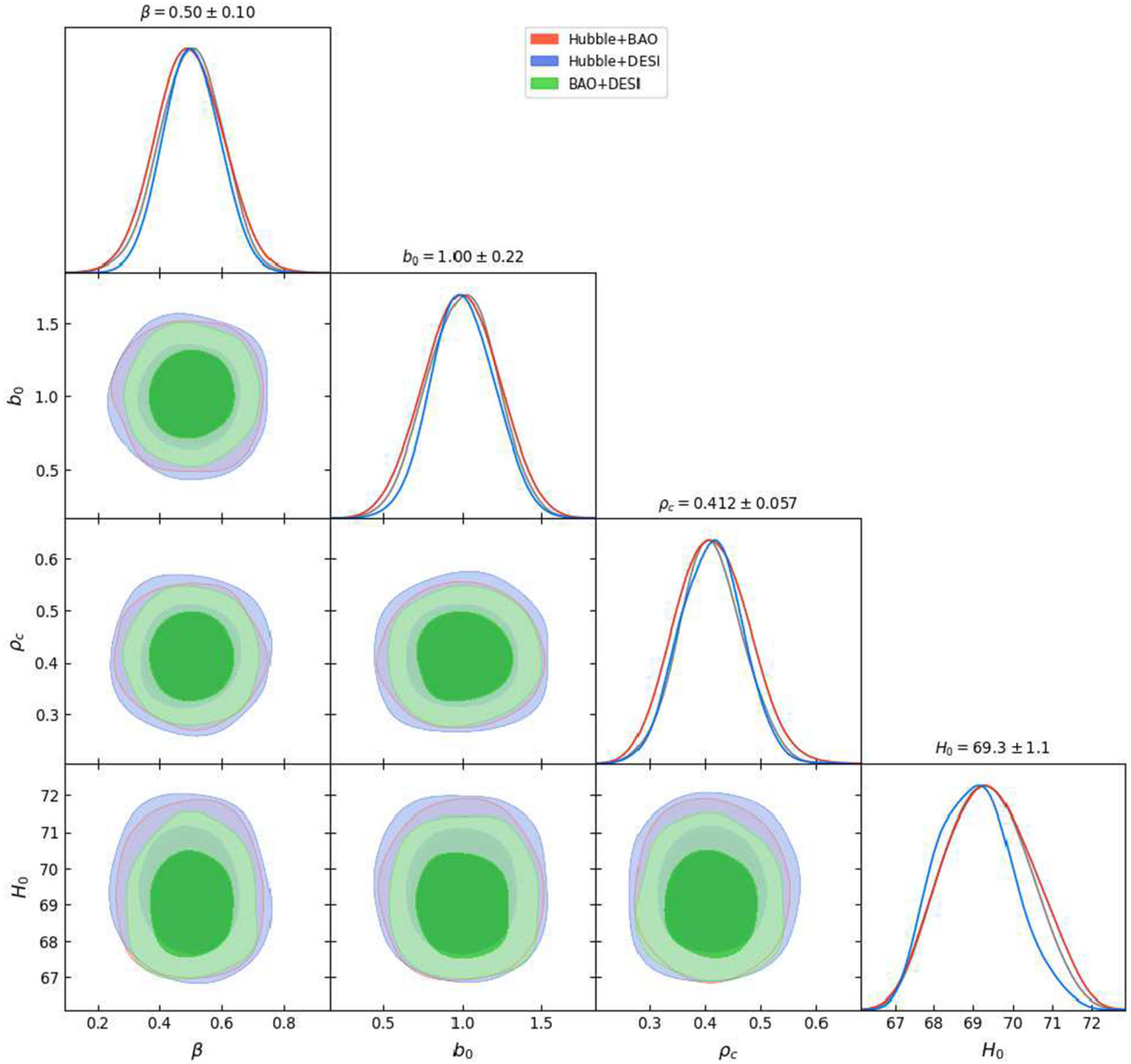

Fig. 12 Joint and marginalized posterior distributions with dataset combination of Hubble+BAO, Hubble+DESI, BAO+DESI, for the non-interacting case. The fixed parameters are considered as $m_{pl} = 1$, $\Omega_{m0} = 0.29$, $n = 1.1$

region of parameter space consistent with the observational data, while the lighter outer contour shows the extended range allowed by the data at a higher uncertainty level. All contour plots in this analysis ensure statistical consistency and reproducibility. The colours were chosen to maintain clarity between the 68% and 95% confidence regions across all.

5.2 Statistical analysis

The model parameters β, b_0, ρ_c, H_0 are constrained using a Markov Chain Monte Carlo (MCMC) approach implemented via the `emcee` sampler [81]. The posterior distributions are visualized using the `GetDist` package [82]. For each dataset and its combinations with other datasets, we compute the best-fit values and corresponding σ confidence intervals (68% $C.L.$). The results are summarized in Tables 1 and Table 2.

The likelihood function is defined as

$$\mathcal{L} \propto \exp\left(-\frac{1}{2}\chi^2\right), \tag{5.1}$$

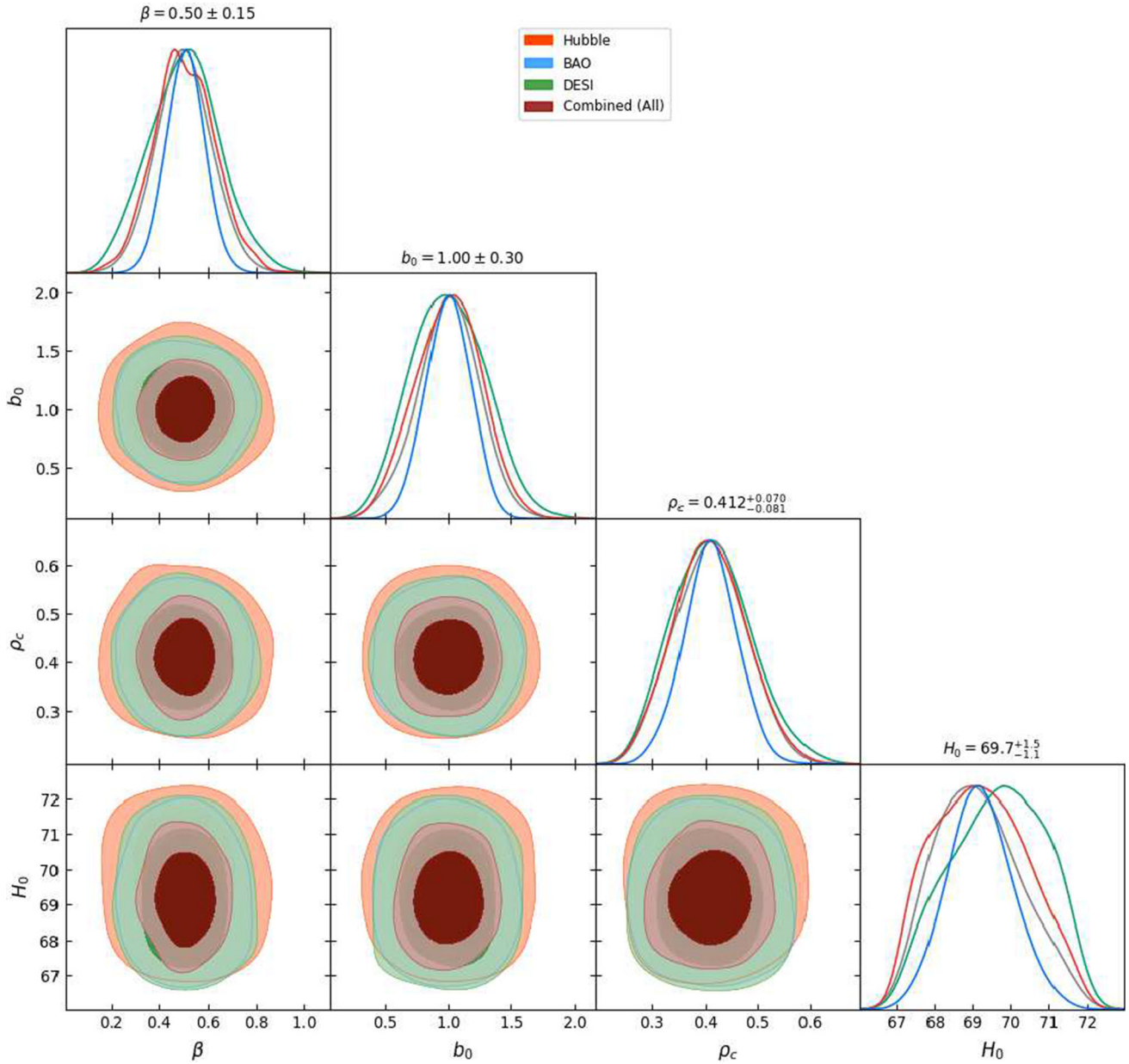

Fig. 13 Joint and marginalized posterior distributions with combinations of datasets Hubble, BAO, DESI and Combined(Hubble+BAO+DESI) for the non-interacting case. The fixed parameters are considered as $m_{pl} = 1$, $\Omega_{m0} = 0.29$, $n = 1.1$

where the Chi-square function is given by

$$\chi^2 = \Delta \mathbf{D}^T \mathbf{C}^{-1} \Delta \mathbf{D}, \tag{5.2}$$

with $\Delta \mathbf{D} = \mathbf{D}_{\rm obs} - \mathbf{D}_{\rm th}$, and $\mathbf{C}$ denoting the covariance matrix for each dataset.

5.3 Parameter constraints

Here, we present the constraints on the free parameter as computed by the data analysis using the MCMC algorithm for different datasets. The results are presented for both the non-interacting and interacting cases separately.

5.3.1 Non-interacting case

The constrained values for the non-interacting case are presented in Table 1. The fixed parameters are considered as $m_{pl} = 1$, $\Omega_{m0} = 0.29$, $n = 1.1$.

The contours showing the joint and the marginalized distributions with the datasets and their combinations are presented in Figs. 11, 12 and 13 for the non-interacting case.

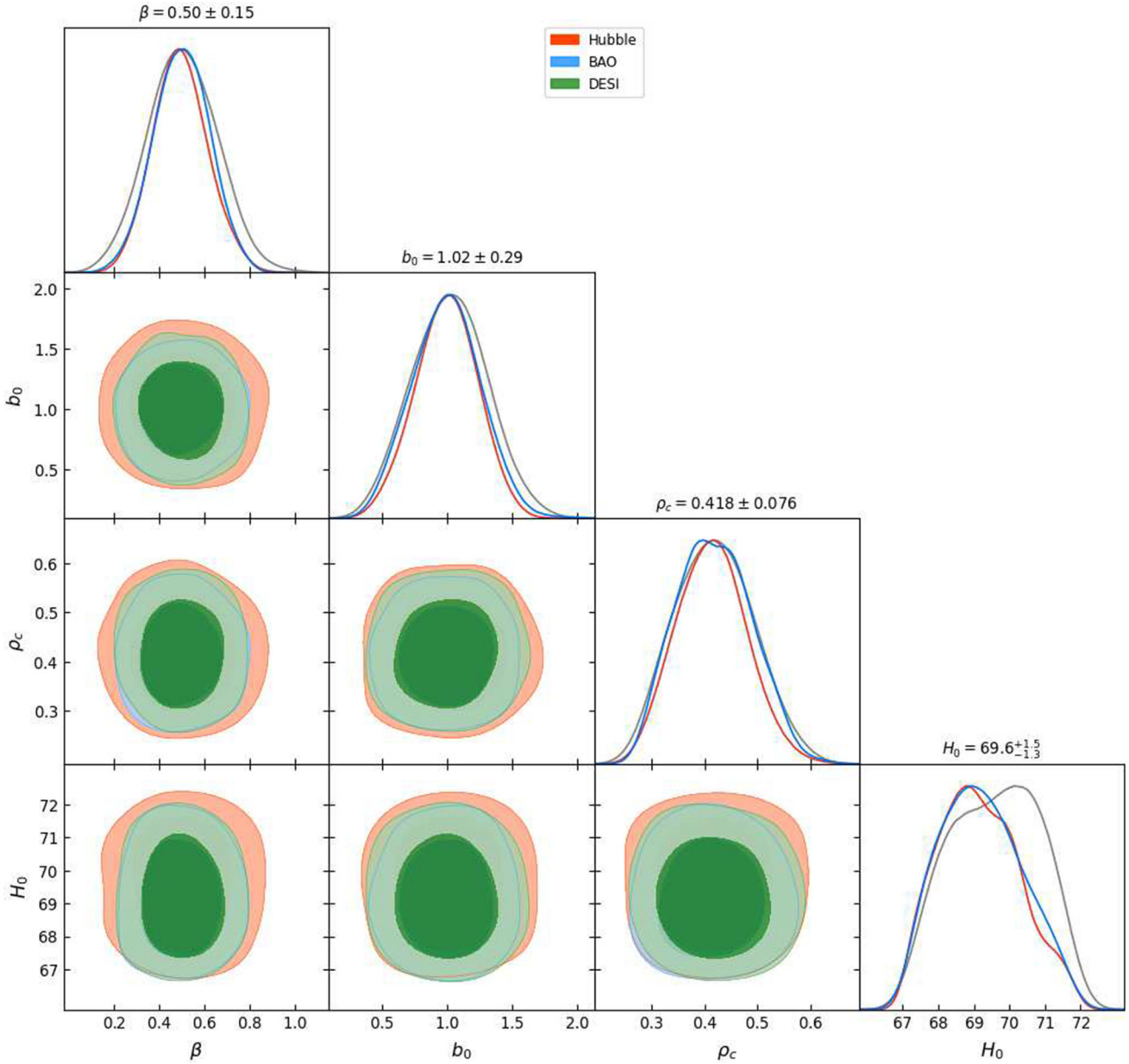

Fig. 14 Joint and marginalized posterior distributions with combinations of datasets Hubble, BAO and DESI for the interacting case. The fixed parameters are considered as $m_{pl} = 1$, $\Omega_{m0} = 0.29$, $n = 1.1$, $\delta = 0.02$

Table 1 Parameter constraints for individual and combined datasets for non interacting case

Dataset	β	H_0 (km s^{-1} Mpc^{-1})	ρ_c	b_0
HUBBLE	0.5034 ± 0.1498	69.6774 ± 1.2518	0.4123 ± 0.0750	1.0041 ± 0.2971
BAO	0.5009 ± 0.1165	69.1494 ± 1.1458	0.4100 ± 0.0680	1.0031 ± 0.2455
DESI	0.5035 ± 0.1267	69.2102 ± 1.2356	0.4095 ± 0.0692	1.0035 ± 0.2605
HUBBLE+BAO	0.5018 ± 0.1006	69.3367 ± 1.0593	0.4116 ± 0.0575	1.0006 ± 0.2186
HUBBLE+DESI	0.4979 ± 0.1081	69.4019 ± 1.1159	0.4131 ± 0.0651	0.9969 ± 0.2345
BAO+DESI	0.5042 ± 0.0903	69.0517 ± 0.9702	0.4116 ± 0.0561	1.0076 ± 0.2008
HUBBLE+BAO+DESI	0.5067 ± 0.0797	69.2016 ± 0.8672	0.4102 ± 0.0511	1.0028 ± 0.1769

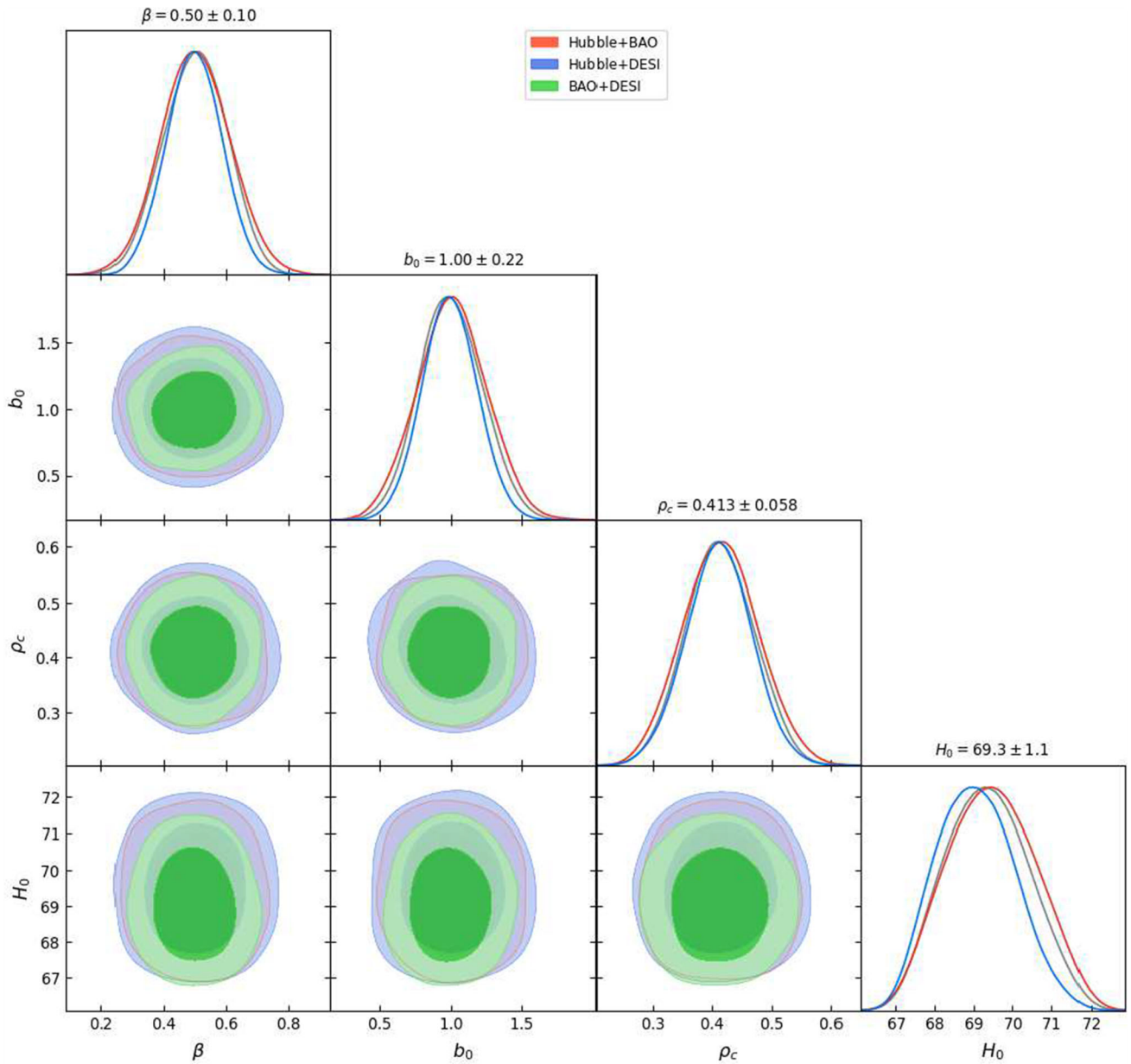

Fig. 15 Joint and marginalized posterior distributions with combinations of datasets combination of Hubble+BAO, Hubble+DESI, BAO+DESI, for the Interacting case. The fixed parameters are considered as $m_{pl} = 1$, $\Omega_{m0} = 0.29$, $n = 1.1$, $\delta = 0.02$

The constrained values obtained for H_0 lie in the acceptable range. Intuitively, the values of the parameters depend on the choice of units. We see that the constrained value of the critical density is obtained as $\rho_c \approx 0.41$. We know that the physical value of the critical density is $\rho_c = 0.41\rho_{pl}$. In Planck units ($c = G = \hbar = 1$) the value of Planck density is $\rho_{pl} = 1$. So in this unit, the critical density $\rho_c \approx 0.41$. This is exactly what we have obtained in our MCMC analysis. This value is physically consistent and therefore eliminates all ambiguity that may arise from scaling and normalization of units. Now it perfectly aligns with the theoretical predictions of LQC.

5.3.2 Interacting case

The constrained values for the interacting case are presented in Table 2. The fixed parameters are considered as $m_{pl} = 1$, $\Omega_{m0} = 0.29$, $n = 1.1$, $\delta = 0.02$. Here also we see that H_0 and ρ_c perfectly lie in the acceptable range.

The contours showing the joint and the marginalized distributions with the datasets and their combinations are presented in Figs. 14, 15 and 16 for the interacting case.

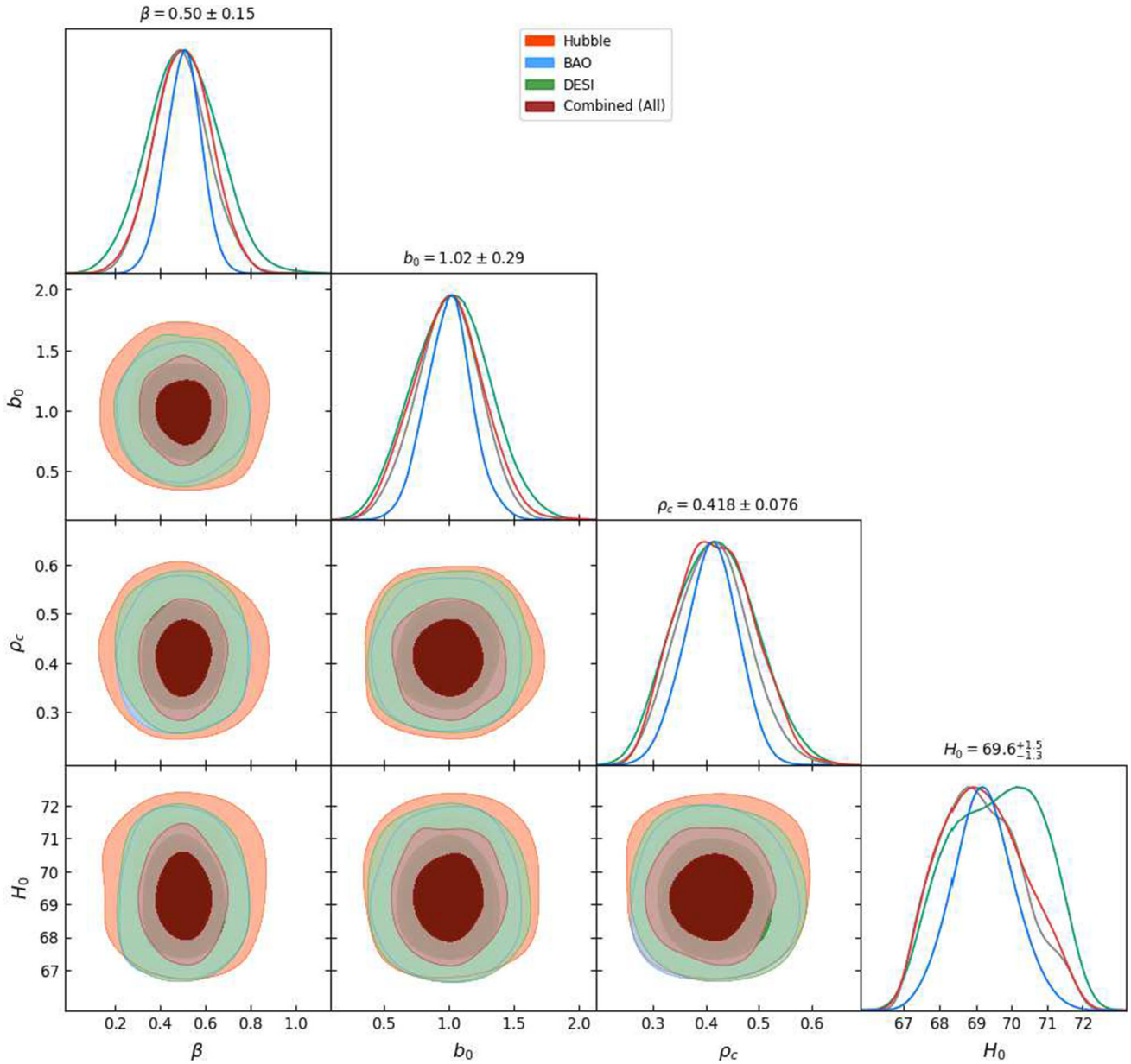

Fig. 16 Joint and marginalized posterior distributions with combinations of datasets Hubble, BAO, DESI and Combined(Hubble+BAO+DESI) for the Interacting case. The fixed parameters are considered as $m_{pl} = 1$, $\Omega_{m0} = 0.29$, $n = 1.1$, $\delta = 0.02$

Table 2 Parameter constraints for individual and combined datasets for interacting case

Dataset	β	H_0 (km s^{-1} Mpc^{-1})	ρ_c	b_0
HUBBLE	0.5040 ± 0.1549	69.6064 ± 1.2852	0.4179 ± 0.0758	1.0195 ± 0.2922
BAO	0.4942 ± 0.1216	69.1576 ± 1.1547	0.4129 ± 0.0668	0.9959 ± 0.2412
DESI	0.5002 ± 0.1240	69.2052 ± 1.1841	0.4183 ± 0.0715	0.9959 ± 0.2658
HUBBLE+BAO	0.5015 ± 0.1021	69.3444 ± 1.0788	0.4129 ± 0.0577	1.0027 ± 0.2214
HUBBLE+DESI	0.5030 ± 0.1108	69.4663 ± 1.1356	0.4142 ± 0.0633	1.0110 ± 0.2448
BAO+DESI	0.4983 ± 0.0889	69.0466 ± 1.0048	0.4111 ± 0.0556	0.9948 ± 0.1924
HUBBLE+BAO+DESI	0.5030 ± 0.0793	69.2343 ± 0.8598	0.4100 ± 0.0503	0.9994 ± 0.1784

6 Discussion and conclusion

In this study, we examine the New Agegraphic Dark Energy (NADE) model within the framework of Loop Quantum Cosmology (LQC), incorporating a quantum gravitational viewpoint into the evolution of dark energy. We have investigated how the discrete quantum geometry of spacetime affects the evolution of NADE and the general cosmic dynamics by integrating the modified Friedmann equations resulting from loop quantum corrections. By using conformal time as the dynamical scale, the NADE model effectively resolves the early-universe inconsistencies of the original agegraphic dark energy scenario and displays rich and feasible cosmological behavior in the LQC environment. Our model considers a combination of cold dark matter and NADE with LQC as the underlying gravity theory. The motivation stems from the quest to understand the quantum origin of cosmic acceleration. While the NADE model connects dark energy to spacetime quantum fluctuations and the conformal age of the universe, it lacks a direct link to quantum gravity. Loop Quantum Gravity (LQG), being a non-perturbative and background-independent approach to spacetime quantization, introduces quantum geometric corrections that influence cosmic evolution. Embedding NADE in the LQG framework enables the investigation of how these quantum effects alter dark energy dynamics, address cosmological singularities, refine late-time acceleration, and offer a consistent quantum-to-classical description of the expansion of the universe.

Both interacting and non-interacting scenarios between dark energy and matter are examined, analyzing key cosmological parameters such as the equation of state, deceleration, and statefinder parameters. The squared speed of sound is evaluated to assess the model's stability. In the non-interacting case, the EoS parameter indicates a quintessence phase for $\frac{1}{2} < \beta < 1$, presents a ΛCDM phase at $\beta = 1$, a phantom phase for $\beta > 1$, and represents pressureless dust at $\beta = \frac{2}{5}$. For the interacting case, the model exhibits quintessence behavior for different values of β. The deceleration parameter q versus redshift z reveals a smooth transition from the decelerating phase to an accelerating phase around $z \approx 0.5$, which is observationally favored. The plots of the squared sound speed confirm classical stability throughout cosmic evolution. The trajectories in the $(r-s)$ plane for various values of β lie within the quintessence region for both interacting and non-interacting models. Observational data are used to constrain the free parameters of the model. Contour plots showing the joint and the marginalized distribution with different datasets are generated and presented in the work. Overall, our findings imply that the interaction of loop quantum effects with agegraphic dark energy offers a non-singular origin scenario and a theoretically sound and observationally compatible explanation of the universe's late-time acceleration. In order to fully explore the phenomenological potential of NADE in the loop quantum cosmology paradigm, future studies may expand this analysis to incorporate interacting agegraphic components, perturbative dynamics, etc.

Acknowledgements PR acknowledges the Inter-University Centre for Astronomy and Astrophysics (IUCAA), Pune, India, for granting a visiting associateship. The authors acknowledge the hospitality provided by IUCAA during a visit, when the majority of this work was done. The authors thank the anonymous referee for his/her constructive comments that helped them to improve the quality of the manuscript.

Funding There is no funding to report for this article.

Data Availability Statement This manuscript has no associated data. [Author's' comment: The data used in the study have been mentioned in the paper. References [74] to [80]].

Code Availability Statement This manuscript has no associated code/software. [Author's comment: Publicly available CosmoMC code has been used during the study. Ref [82] https://cosmologist.info/cosmomc/.]

Declarations

Conflict of interest There are no conflict of interest.

Funded by SCOAP[3].

References

1. S. Perlmutter et al., Discovery of a supernova explosion at half the age of the universe and its cosmological implications. Nature **391**, 51–54 (1998). https://doi.org/10.1038/34124. arXiv:astro-ph/9712212
2. S. Perlmutter et al., Measurements of Ω and Λ from 42 high redshift supernovae. Astrophys. J. **517**, 565–586 (1999). https://doi.org/10.1086/307221. arXiv:astro-ph/9812133
3. A.G. Riess et al., Observational evidence from supernovae for an accelerating universe and a cosmological constant. Astron. J. **116**, 1009–1038 (1998). https://doi.org/10.1086/300499. arXiv:astro-ph/9805201
4. D.N. Spergel et al., First year Wilkinson Microwave Anisotropy Probe (WMAP) observations: determination of cosmological parameters. Astrophys. J. Suppl. **148**, 175–194 (2003). https://doi.org/10.1086/377226. arXiv:astro-ph/0302209
5. E. Komatsu et al., Five-Year Wilkinson Microwave Anisotropy Probe (WMAP) observations: cosmological interpretation. Astrophys. J. Suppl. **180**, 330–376 (2009). https://doi.org/10.1088/0067-0049/180/2/330. arXiv:0803.0547
6. D.J. Eisenstein, W. Hu, Baryonic features in the matter transfer function. Astrophys. J. **496**, 605 (1998). https://doi.org/10.1086/305424. arXiv:astro-ph/9709112

7. D.J. Eisenstein et al., Detection of the baryon acoustic peak in the large-scale correlation function of SDSS Luminous Red Galaxies. Astrophys. J. **633**, 560–574 (2005). https://doi.org/10.1086/466512. arXiv:astro-ph/0501171
8. T. Barreiro, O. Bertolami, P. Torres, Wmap five-year data constraints on the unified model of dark energy and dark matter. Phys. Rev. D **78**(4), 043530 (2008)
9. P. Brax, What makes the Universe accelerate? A review on what dark energy could be and how to test it. Rep. Prog. Phys. **81**(1), 016902 (2018). https://doi.org/10.1088/1361-6633/aa8e64
10. S. Nojiri, S.D. Odintsov, Unifying phantom inflation with late-time acceleration: scalar phantom–non-phantom transition model and generalized holographic dark energy. Gen. Relativ. Gravit. **38**(8), 1285–1304 (2006). https://doi.org/10.1007/s10714-006-0301-6
11. M. Li, A model of holographic dark energy. Phys. Lett. B **603**, 1 (2004). https://doi.org/10.1016/j.physletb.2004.10.014. arXiv:hep-th/0403127
12. S. Wang, Y. Wang, M. Li, Holographic dark energy. Phys. Rep. **696**, 1–57 (2017). https://doi.org/10.1016/j.physrep.2017.06.003. arXiv:1612.00345
13. R.-G. Cai, A dark energy model characterized by the age of the universe. Phys. Lett. B **657**(4–5), 228–231 (2007). https://doi.org/10.1016/j.physletb.2007.09.061
14. I.P. Neupane, A note on agegraphic dark energy. Phys. Lett. B **673**, 111–118 (2009). https://doi.org/10.1016/j.physletb.2009.02.012. arXiv:0708.2910
15. S. Weinberg, The cosmological constant problem. Rev. Mod. Phys. **61**, 1–23 (1989). https://doi.org/10.1103/RevModPhys.61.1
16. T. Padmanabhan, Cosmological constant: the weight of the vacuum. Phys. Rep. **380**, 235–320 (2003). https://doi.org/10.1016/S0370-1573(03)00120-0. arXiv:hep-th/0212290
17. J. Garriga, A. Vilenkin, On likely values of the cosmological constant. Phys. Rev. D **61**, 083502 (2000). https://doi.org/10.1103/PhysRevD.61.083502
18. S.A. Bludman, Vacuum energy: if not now, then when? Nucl. Phys. A **663–664**, 865c–868c (2000). https://doi.org/10.1016/S0375-9474(99)00733-2
19. J. Garriga, A. Vilenkin, Solutions to the cosmological constant problems. Phys. Rev. D **64**, 023517 (2001). https://doi.org/10.1103/PhysRevD.64.023517
20. P. Rudra, Does $f(R, T)$ gravity admit a stationary scenario between dark energy and dark matter in its framework? Eur. Phys. J. Plus **130**(4), 66 (2015). https://doi.org/10.1140/epjp/i2015-15066-8. arXiv:1502.06861
21. P. Rudra, Towards a possible solution for the coincidence problem: f(G) gravity as background. Int. J. Mod. Phys. D **24**(02), 1550013 (2014). https://doi.org/10.1142/S0218271815500133. arXiv:1411.3583
22. P. Rudra, Coincidence problem in f(T) gravity models. Astrophys. Space Sci. **357**(2), 135 (2015). https://doi.org/10.1007/s10509-015-2365-9. arXiv:1410.6710
23. F. Károlyházy, On the structure of space-time. Il Nuovo Cimento A **42**(2), 390–402 (1966). (**originally in Hungarian; English translation or summary often cited**)
24. F. Károlyházy, P. Lúkács, A tentative expression of the Károlyházy uncertainty of the space-time structure through vacuum spreads in quantum gravity. Phys. Bull. **33**(1), 1–8 (1982). (**often cited in later agegraphic dark energy works**)
25. F. Károlyházy, Quantum fluctuations of space-time and the theory of gravitation. Nuovo Cimento B **79**(1), 1–12 (1986)
26. M. Maziashvili, Space–time in light of károlyházy uncertainty relation (2006). arXiv preprintV2 arXiv:gr-qc/0612110
27. M. Maziashvili, Cosmological implications of Károlyházy uncertainty relation. Int. J. Mod. Phys. D **16**(9), 1531–1539 (2007). https://doi.org/10.1142/S0218271807011182
28. N. Sasakura, An uncertainty relation of space–time (1999). arXiv preprint. arXiv:hep-th/9903146
29. H. Wei, R.-G. Cai, A new model of agegraphic dark energy. Phys. Lett. B **660**(3), 113–117 (2008). https://doi.org/10.1016/j.physletb.2007.12.030
30. H. Wei, R.-G. Cai, Cosmological constraints on new agegraphic dark energy. Phys. Lett. B **663**(1–2), 1–6 (2008). https://doi.org/10.1016/j.physletb.2008.03.048
31. H. Wei, R.-G. Cai, Cosmological constraints on new agegraphic dark energy. Phys. Lett. B **663**(1), 1–6 (2008)
32. J. Zhang, L. Zhang, X. Zhang, Sandage–Loeb test for the new agegraphic and Ricci dark energy models. Phys. Lett. B **691**, 11–17 (2010). https://doi.org/10.1016/j.physletb.2010.06.013. arXiv:1006.1738
33. J.-F. Zhang, Y.-H. Li, X. Zhang, A global fit study on the new agegraphic dark energy model. Eur. Phys. J. C (2013). https://doi.org/10.1140/epjc/s10052-013-2280-6
34. L. Xiang-Lai, Z. Xin, New agegraphic dark energy in Brans–Dicke theory. Commun. Theor. Phys. **52**(4), 761–768 (2009). https://doi.org/10.1088/0253-6102/52/4/37
35. X.-L. Liu, J. Zhang, X. Zhang, Theoretical limits on agegraphic quintessence from weak gravity conjecture. Phys. Lett. B **689**(4), 139–144 (2010)
36. Y.-H. Li, J.-F. Zhang, X. Zhang, New initial condition of the new agegraphic dark energy model. Chin. Phys. B **22**(3), 039501 (2013). https://doi.org/10.1088/1674-1056/22/3/039501
37. P. Saha, S. Maity, U. Debnath, Reconstructing extended f(P) cubic gravity from entropy-corrected holographic and new agegraphic dark energy models. Mod. Phys. Lett. A **37**(30), 2250204 (2022). https://doi.org/10.1142/S0217732322502042
38. S. Maity, M. Biswas, U. Debnath, Analysis of entropy corrected holographic and new agegraphic dark energy models in generalized Rastall gravity. Int. J. Mod. Phys. A **35**(28), 2050175 (2020). https://doi.org/10.1142/S0217751X20501754
39. S. Maity, U. Debnath, Tsallis, Rényi and Sharma–Mittal holographic and new agegraphic dark energy models in D-dimensional fractal universe. Eur. Phys. J. Plus **134**(10), 514 (2019). https://doi.org/10.1140/epjp/i2019-12884-6
40. H. Hossienkhani, Thermodynamics of interacting new agegraphic dark energy and dark matter due to Bianchi type I model. Int. J. Theor. Phys. **55**(11), 4924–4935 (2016). https://doi.org/10.1007/s10773-016-3117-5
41. M. Sharif, M. Ajmal, Non-interacting new agegraphic dark energy model in f(Q) gravity. High Energy Dens. Phys. **56**, 101198 (2025). https://doi.org/10.1016/j.hedp.2025.101198
42. M. Sharif, E.M. Moneer, I. Ibrar, E.E. Zotos, Investigating cosmic evolution through the new agegraphic dark energy model in $f(Q, \mathbb{T})$ gravity. Pramana **99**(2), 56 (2025). https://doi.org/10.1007/s12043-025-02906-7
43. J.-F. Zhang, Y.-H. Li, X. Zhang, A global fit study on the new agegraphic dark energy model. Eur. Phys. J. C **73**(1), 2280 (2013). https://doi.org/10.1140/epjc/s10052-013-2280-6. arXiv:1212.0300
44. M. Bojowald, Loop quantum cosmology. I. Kinematics. Class. Quantum Gravity **17**, 1489–1508 (2000). https://doi.org/10.1088/0264-9381/17/6/312. arXiv:gr-qc/9910103
45. M. Bojowald, Loop quantum cosmology. II. Volume operators. Class. Quantum Gravity **17**, 1509–1526 (2000). https://doi.org/10.1088/0264-9381/17/6/313. arXiv:gr-qc/9910104
46. C. Rovelli, Loop quantum gravity. Living Rev. Relativ. **11**, 5 (2008). https://doi.org/10.12942/lrr-2008-5
47. A. Ashtekar, E. Bianchi, A short review of loop quantum gravity. Rep. Prog. Phys. **84**(4), 042001 (2021). https://doi.org/10.1088/1361-6633/abed91. arXiv:2104.04394

48. A. Ashtekar, J. Lewandowski, Background independent quantum gravity: a status report. Class. Quantum Gravity **21**(15), R53–R152 (2004). https://doi.org/10.1088/0264-9381/21/15/r01
49. W. Zimdahl, Interacting dark energy and cosmological equations of state. Int. J. Mod. Phys. D **14**(12), 2319–2325 (2005). https://doi.org/10.1142/S0218271805007784
50. S. Maity, U. Debnath, Generalized ghost version of pilgrim dark energy in loop quantum gravity motivated cosmology. Gravit. Cosmol. **27**(4), 375–382 (2021). https://doi.org/10.1134/S0202289321040095
51. B. Elizaga Navascués, On the evolution of the volume in Loop Quantum Cosmology. Class. Quantum Gravity **41**(14), 145004 (2024). https://doi.org/10.1088/1361-6382/ad56ee. arXiv:2311.18066
52. C.-Y. Lin, X. Liu, Y. Ma, C. Zhang, Conformally invariant Brans–Dicke loop quantum cosmology: a quantum geometric model of linking theory. Phys. Rev. D **108**(12), 124074 (2023). https://doi.org/10.1103/PhysRevD.108.124074. arXiv:2307.11222
53. M. Bruno, G. Montani, Is the diagonal case a general picture for loop quantum cosmology? Phys. Rev. D **108**(4), 046003 (2023). https://doi.org/10.1103/PhysRevD.108.046003. arXiv:2306.10934
54. S. Noori Gashti, İ Sakallı, H. Farahani, P. Rudra, B. Pourhassan, Impact of loop quantum gravity on the topological classification of quantum-corrected black holes. Universe **11**(8), 247 (2025). https://doi.org/10.3390/universe11080247
55. B. ElizagaNavascués, G.A. MenaMarugán, A.M. Sánchez, Extended phase space quantization of a black hole interior model in loop quantum cosmology. Phys. Rev. D **108**(10), 106001 (2023). https://doi.org/10.1103/PhysRevD.108.106001. arXiv:2306.06090
56. R. Chowdhury, P. Rudra, Interacting generalised cosmic Chaplygin gas in loop quantum cosmology: a singularity free universe. Int. J. Theor. Phys. **52**, 489–503 (2013). https://doi.org/10.1007/s10773-012-1353-x. arXiv:1204.3531
57. S. Nojiri, S.D. Odintsov, H. Štefančić, Transition from a matter-dominated era to a dark energy universe. Phys. Rev. D **74**, 086009 (2006). https://doi.org/10.1103/PhysRevD.74.086009
58. T. Mukhopadhyay, B. Chakraborty, A. Kotal, U. Debnath, Reconstructions of f($\mathscr{P}$)Lg and f($\mathscr{Q}$)Lg gravity models from (m, n)Lg-type Barrow Holographic Dark Energy: Analysis and Observational Constraints. Int. J. Geom. Methods Mod. Phys. **22**(08), 2550051 (2025). https://doi.org/10.1142/S0219887825500513
59. Z.-H. Zhu, M. Hu, J. Alcaniz, Y.-X. Liu, Testing power-law cosmology with galaxy clusters. Astron. Astrophys. **483**(1), 15–18 (2008). https://doi.org/10.1051/0004-6361:20077797 (scale factor $a(t) \propto t^{\alpha}$ with $\alpha \gtrsim 1$)
60. S. Kumar, Observational constraints on Hubble constant and deceleration parameter in power-law cosmology. Mon. Not. R. Astron. Soc. **422**(3), 2532–2538 (2012). using $a(t) \propto t^{\alpha}$ and constraining via $H(z)$ SNeIa. https://doi.org/10.1111/j.1365-2966.2012.20810.x
61. M. Sharif, S. Waheed, Cosmic evolution in self-interacting brans–dicke cosmology, arXiv e-printAssumes power-law for scalar field and scale factor in Bianchi I model (2012). arXiv:arXiv:1211.3795
62. J. Singh, Shaily, A. Pradhan, A. Beesham, Power law cosmology in modified theory with thermodynamics analysis, arXiv e-printPower-law scale factor in $f(R, G)$ gravity and observational fits (2023). arXiv:arXiv:2304.09917
63. W. Yang, S. Pan, J.D. Barrow, Large-scale stability and astronomical constraints for coupled dark-energy models. Phys. Rev. D **97**, 043529 (2018). https://doi.org/10.1103/PhysRevD.97.043529
64. S.D. Odintsov, V.K. Oikonomou, P.V. Tretyakov, Phase space analysis of the accelerating multifluid universe. Phys. Rev. D **96**, 044022 (2017). https://doi.org/10.1103/PhysRevD.96.044022
65. S.D. Odintsov, V.K. Oikonomou, Study of finite-time singularities of loop quantum cosmology interacting multifluids. Phys. Rev. D **97**, 124042 (2018). https://doi.org/10.1103/PhysRevD.97.124042
66. S. Nojiri, S.D. Odintsov, Unified cosmic history in modified gravity: from theory to Lorentz non-invariant models. Phys. Rep. **505**(2–4), 59–144 (2011). https://doi.org/10.1016/j.physrep.2011.04.001
67. S. Nojiri, S. Odintsov, V. Oikonomou, Modified gravity theories on a nutshell: inflation, bounce and late-time evolution. Phys. Rep. **692**, 1–104 (2017). https://doi.org/10.1016/j.physrep.2017.06.001
68. Z.-K. Guo, N. Ohta, S. Tsujikawa, Probing the coupling between dark components of the universe. Phys. Rev. D **76**, 023508 (2007). https://doi.org/10.1103/PhysRevD.76.023508
69. P. Singh, Loop cosmological dynamics and dualities with Randall–Sundrum braneworlds. Phys. Rev. D **6**, 73 (2006). https://doi.org/10.1103/physrevd.73.063508
70. H.-H. Xiong, J.-Y. Zhu, Tachyon field in loop quantum cosmology: inflation and evolution picture. Phys. Rev. D **75**, 084023 (2007). https://doi.org/10.1103/PhysRevD.75.084023
71. B.-F. Li, P. Singh, A. Wang, Qualitative dynamics and inflationary attractors in loop cosmology. Phys. Rev. D **6**, 98 (2018). https://doi.org/10.1103/physrevd.98.066016
72. V. Sahni, T.D. Saini, A.A. Starobinsky, U. Alam, Statefinder: a new geometrical diagnostic of dark energy. JETP Lett. **77**, 201–206 (2003). https://doi.org/10.1134/1.1574831. arXiv:astro-ph/0201498
73. U. Alam, V. Sahni, T.D. Saini, A.A. Starobinsky, Exploring the expanding universe and dark energy using the Statefinder diagnostic. Mon. Not. R. Astron. Soc. **344**, 1057 (2003). https://doi.org/10.1046/j.1365-8711.2003.06871.x. arXiv:astro-ph/0303009
74. R. Jimenez, A. Loeb, Constraining cosmological parameters based on relative galaxy ages. Astrophys. J. **573**, 37–42 (2002). https://doi.org/10.1086/340549. arXiv:astro-ph/0106145
75. M. Moresco, Raising the bar: new constraints on the Hubble parameter with cosmic chronometers at z 2. Mon. Not. R. Astron. Soc. **450**(1), L16–L20 (2015). https://doi.org/10.1093/mnrasl/slv037. arXiv:1503.01116
76. M. Moresco, A. Cimatti, R. Jimenez, L. Pozzetti, G. Zamorani, M. Bolzonella, P. Rosati et al., Improved constraints on the expansion rate of the Universe up to z 1.1 from the spectroscopic evolution of cosmic chronometers. JCAP **08**, 006 (2012). https://doi.org/10.1088/1475-7516/2012/08/006. arXiv:1201.3609
77. M. Moresco, L. Pozzetti, A. Cimatti, R. Jimenez, C. Maraston, L. Verde, D. Thomas et al., A 6% measurement of the Hubble parameter at $z \sim 0.45$: direct evidence of the epoch of cosmic re-acceleration. JCAP **05**, 014 (2016). https://doi.org/10.1088/1475-7516/2016/05/014. arXiv:1601.01701
78. DESI, I: Overview of the Dark Energy Spectroscopic Instrument (DESI) and its cosmological measurements. Astrophys. J. Suppl. **269**(2024), 6 (2024). https://doi.org/10.3847/1538-4365/ad2e19. arXiv:2404.03000
79. S. Alam, M. Aubert, S. Avila, C. Balland, J.E. Bautista et al., Completed SDSS-IV extended Baryon Oscillation Spectroscopic Survey: cosmological implications from two decades of spectroscopic surveys at the Apache Point Observatory. Phys. Rev. D **103**(8), 083533 (2021). https://doi.org/10.1103/PhysRevD.103.083533. arXiv:2007.08991
80. DESI 2025 II: Baryon Acoustic Oscillation and Redshift-Space Distortion Measurements from the DESI Survey (2025). arXiv:2501.00000
81. D. Foreman-Mackey, D.W. Hogg, D. Lang, J. Goodman, emcee: The MCMC Hammer. Publ. Astron. Soc. Pac. **125**, 306 (2013). https://doi.org/10.1086/670067. arXiv:1202.3665
82. A. Lewis, GetDist: a Python package for analysing Monte Carlo samples (2019). arXiv:1910.13970